Chapter 8

Bioconvective stagnation-point flow over a rotating stretchable disk *

8.1 Introduction

The striking point at which the fluid's local velocity is zero is denominated as the stagnation-point. The phenomenon caused by the unpredictable movement of microorganisms is termed bioconvection. Owing to its practical application in pharmaceuticals, biosensors, medical instruments, bio-chromatography, microchip pump, biomedical science, micro-actuators, and aerodynamics, the bioconvective stagnation-point flow over a whirling extendible disk is investigated. Ferro-nanofluid has been particularly chosen in this work since water-based magnetite nanofluid and rotating disk share similar applications. The nanomaterial flow has been modelled using the modified Buongiorno nanofluid model (MBNM). The impact of the stratification constraints and magnetic field are also accounted. Von Kármán's similarity transformations are employed and the transmuted nonlinear ODEs are resolved using the finite-difference based *bvp5c* routine. MATLAB generated flow profiles have been analyzed for augmentations in the influential parameter values. The influence of magnetic field parameter ($0.2 \leq M \leq 1.8$), thermal stratification parameter ($0.1 \leq S_1 \leq 0.5$), volume fraction of magnetite nanoparticles ($0.01 \leq \phi \leq 0.09$), and velocity ratio parameter ($0.1 \leq S \leq 0.5$) on the heat transfer rate has been scrutinized statistically using a five-level four-factor response surface optimized model. The main objectives of the current chapter are to:

*Published in: Journal of the Indian Chemical Society (Elsevier), 2022; 99(8); 100615.

- Model the bioconvective stagnation-point flow of ferro-nanofluid over a rotating stretchable disk using the modified Buongiorno nanofluid model.
- Analyze the MATLAB generated flow profiles for augmentations in the effectual parameter values.
- Depict the simultaneous effect of influential parameters on the physical quantities with the aid of three-dimensional surface plots.
- Estimate the interactive effects of the key parameters on the heat transfer rate utilizing the five-level four-factor response surface optimized model.

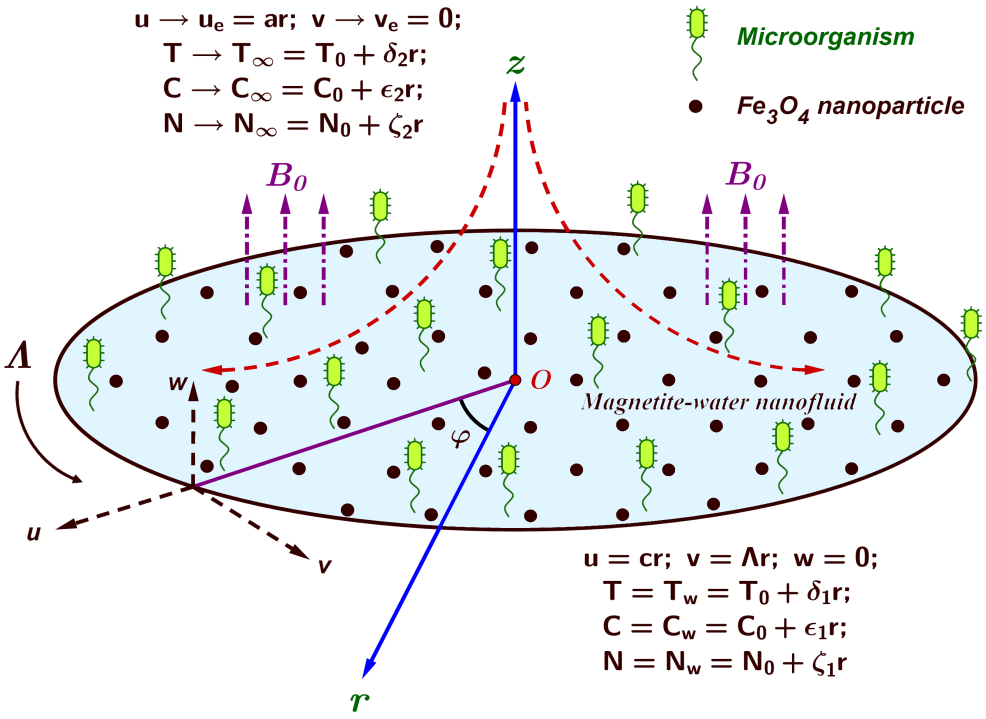

Figure 8.1: Geometrical Frame

8.2 Mathematical Frame

Consider an incompressible, steady and axisymmetric stagnation-point flow of water-based magnetite nanofluid containing gyrotactic microorganisms past a circular disk with a stretching velocity, cr and a constant angular velocity, Λ that imparts swirling flow in the neighbouring fluid layers (see Figure 8.1). The velocity components (u, v, w) denotes the nanofluid flow in the radial (r), azimuthal (φ), and

axial (z) directions, respectively. An external magnetic field (of uniform intensity B_0) is applied along the axial direction. Let ($T,\ T_0,\ T_w,\ T_\infty$) denote the nanomaterial temperature, the reference temperature, the temperature at the disk, and the ambient temperature, respectively. Let ($C,\ C_0,\ C_w,\ C_\infty$) indicate the nanoparticle volume fraction, the reference nanoparticle volume fraction, the nanoparticle volume fraction at the disk, and the ambient nanoparticle volume fraction, correspondingly and also let ($N,\ N_0,\ N_w,\ N_\infty$) denote the microbial concentration, the reference microbial concentration, the microbial concentration at the disk, and the ambient microbial concentration, respectively. The effects of Joule heating and viscous dissipation are negligible and hence not considered. The thermal, solutal, and motile density stratification constraints and linear chemical reaction effects are also incorporated. The induced magnetic field has been neglected due to the assumption of a small magnetic Reynolds number.

Following the two-phase MBNM and the aforementioned assumptions, the governing equations take the form (see Mustafa et al., 2016; Waqas et al., 2021):

$$\frac{\partial u}{\partial r}+\frac{u}{r}+\frac{\partial w}{\partial z}=0 \tag{8.2.1}$$

$$u\frac{\partial u}{\partial r}-\frac{v^2}{r}+w\frac{\partial u}{\partial z}=u_e\frac{du_e}{dr}+\left(\frac{\mu_{nf}}{\rho_{nf}}\right)\frac{\partial^2 u}{\partial z^2}-\left(\frac{\sigma_{nf}}{\rho_{nf}}\right)B_o^2\left(u-u_e\right) \tag{8.2.2}$$

$$u\frac{\partial v}{\partial r}+\frac{uv}{r}+w\frac{\partial v}{\partial z}=\left(\frac{\mu_{nf}}{\rho_{nf}}\right)\frac{\partial^2 v}{\partial z^2}-\left(\frac{\sigma_{nf}}{\rho_{nf}}\right)B_o^2 v \tag{8.2.3}$$

$$u\frac{\partial T}{\partial r}+w\frac{\partial T}{\partial z}=\frac{k_{nf}}{\left(\rho C_p\right)_{nf}}\ \frac{\partial^2 T}{\partial z^2}+\frac{\left(\rho C_p\right)_p}{\left(\rho C_p\right)_{nf}}\left(D_B\left(\frac{\partial T}{\partial z}\frac{\partial C}{\partial z}\right)+\frac{D_T}{T_\infty}\left(\frac{\partial T}{\partial z}\right)^2\right) \tag{8.2.4}$$

$$u\frac{\partial C}{\partial r}+w\frac{\partial C}{\partial z}=D_B\frac{\partial^2 C}{\partial z^2}+\frac{D_T}{T_\infty}\ \frac{\partial^2 T}{\partial z^2}-k_r\left(C-C_\infty\right) \tag{8.2.5}$$

$$u\frac{\partial N}{\partial r}+w\frac{\partial N}{\partial z}+\frac{bW_c}{C_w-C_0}\left(\frac{\partial}{\partial z}\left(N\frac{\partial C}{\partial z}\right)\right)=D_m\frac{\partial^2 N}{\partial z^2} \tag{8.2.6}$$

subject to the boundary conditions (see Mustafa et al., 2016; Waqas et al., 2021):

$$u=cr,\ v=\Lambda \mathrm{r}\ ,\ w=0,\ T=T_w=T_0+\delta_1 r,$$
$$C=C_w=C_0+\epsilon_1 r,\ N=N_w=N_0+\zeta_1 r;\ \text{ at } z=0.$$
$$u\to u_e=ar,\ v\to v_e=0,\ T\to T_\infty=T_0+\delta_2 r,$$

$$C \to C_\infty = C_0 + \epsilon_2 r,\ N \to N_\infty = N_0 + \zeta_2 r;\ \text{ as } z \to \infty.$$

where D_B is the Brownian diffusion coefficient, D_T is the thermophoresis diffusion coefficient, D_m is the microorganism diffusion coefficient, and $(u_e,\ v_e)$ are the free stream velocities along $(r,\ \varphi)$ directions.
Consider the following similarity transformations (see Mustafa et al., 2016; Waqas et al., 2021):

$$\eta = \left(\tfrac{c}{\vartheta_f}\right)^{\frac{1}{2}} z,\ u = cr\ F(\eta),\ v = cr\ G(\eta),\ w = (c\vartheta_f)^{\frac{1}{2}}\ H(\eta),$$

$$\theta(\eta) = \frac{T - T_\infty}{T_w - T_0},\ \psi(\eta) = \frac{C - C_\infty}{C_w - C_0},\ \chi(\eta) = \frac{N - N_\infty}{N_w - N_0}$$

Employing the similarity transformations into Equations (8.2.1) – (8.2.6), we get:

$$H' = -2F \tag{8.2.7}$$

$$F'' = \left(\frac{A_2}{A_1}\right)\left(F^2 - G^2 - S^2 + HF'\right) + \left(\frac{A_3}{A_1}\right) M\ (F - S) \tag{8.2.8}$$

$$G'' = \left(\frac{A_2}{A_1}\right)(2FG + HG') + \left(\frac{A_3}{A_1}\right) M\ G \tag{8.2.9}$$

$$\theta'' = \left(\frac{Pr}{A_4}\right)\left(A_5\ H\theta' - Nb\ \theta'\ \psi' - Nt\ (\theta')^2\right) \tag{8.2.10}$$

$$\psi'' = Le\ Pr\ H\psi' + Le\ Pr\ Kr\ \psi - \left(\frac{Nt}{Nb}\right)\theta'' \tag{8.2.11}$$

$$\chi'' = Lb\ Pr\ H\chi' + Pe\ ((\chi + \Omega)\psi'' + \psi'\ \chi') \tag{8.2.12}$$

subject to the boundary conditions

$$F(0) = 1,\ G(0) = \omega\ ,\ H(0) = 0,\ \theta(0) = 1 - S_1,\ \psi(0) = 1 - S_2,$$
$$\chi(0) = 1 - S_3,\ F(\infty) \to S,\ G(\infty) \to 0,\ \theta(\infty) \to 0,\ \psi(\infty) \to 0,\ \chi(\infty) \to 0.$$

where the dimensionless parameters are given in appendix I.

The nanofluid models incorporated are (see Alghamdi et al., 2021):

Effective Dynamic Viscosity : $\dfrac{\mu_{nf}}{\mu_f} = \dfrac{1}{(1-\phi)^{2.5}} = A_1$

Effective Density : $\dfrac{\rho_{nf}}{\rho_f} = (1-\phi) + \phi\left(\dfrac{\rho_{np}}{\rho_f}\right) = A_2$

Effective Specific Heat : $\dfrac{(\rho C_p)_{nf}}{(\rho C_p)_f} = (1-\phi) + \phi\left(\dfrac{(\rho C_p)_{np}}{(\rho C_p)_f}\right) = A_3$

Effective Thermal Conductivity : $\dfrac{k_{nf}}{k_f} = \dfrac{k_{np} + 2k_f - 2\phi\,(k_f - k_{np})}{k_{np} + 2k_f + \phi\,(k_f - k_{np})} = A_4$

Effective Electrical Conductivity : $\dfrac{\sigma_{nf}}{\sigma_f} = 1 + \dfrac{3\left(\frac{\sigma_{np}}{\sigma_f} - 1\right)\phi}{\left(\frac{\sigma_{np}}{\sigma_f} + 2\right) - \left(\frac{\sigma_{np}}{\sigma_f} - 1\right)\phi} = A_5$

The physical quantities are given by (see Turkyilmazoglu, 2012; Mustafa et al., 2016):

Local drag coefficient : $C_f = \dfrac{\sqrt{{\tau_r}^2 + {\tau_\varphi}^2}}{\rho_f (cr)^2}$

$where\ \tau_r = \mu_{nf}\ \left.\dfrac{\partial u}{\partial z}\right|_{z=0}$ and $\tau_\varphi = \mu_{nf}\ \left.\dfrac{\partial v}{\partial z}\right|_{z=0}$

$\Rightarrow\ C_f\ Re^{1/2} = A_1\ \sqrt{(F\,'(0))^2 + (G\,'(0))^2}$

Local Nusselt number : $Nu_r = \dfrac{r q_w}{k_f\,(T_w - T_0)}$

$where\ q_w = -k_{nf}\ \left.\dfrac{\partial T}{\partial z}\right|_{z=0}$

$\Rightarrow\ Nu_r\ Re^{-1/2} = -A_4\ \theta\,'(0)$

Local Sherwood number : $Sh_r = \dfrac{r q_m}{D_B\,(C_w - C_0)}$

$$where\ q_m = -D_B\ \left.\frac{\partial C}{\partial z}\right|_{z=0}$$

$$\Rightarrow\ Sh_r\ Re^{-1/2} = -\psi\,'(0)$$

Local motile density number : $Nn_r = \dfrac{r q_n}{D_m\,(N_w - N_0)}$

$$where\ q_n = -D_m\ \left.\frac{\partial N}{\partial z}\right|_{z=0}$$

$$\Rightarrow\ Nn_r\ Re^{-1/2} = -\chi\,'(0)$$

where $Re = \frac{cr^2}{\vartheta_f}$ is the local Reynold's number.

8.3 Numerical Frame & Validation

Equations (8.2.7) - (8.2.12) together with the boundary conditions are numerically resolved in MATLAB employing the *bvp5c* routine. This is accomplished by initially assuming:

$$F = I_1,\ F\,' = I_2,\ F\,'' = I_2^{'},\ G = I_3,\ G\,' = I_4,\ G\,'' = I_4^{'},$$
$$H = I_5,\ H\,' = I_5^{'},\ \theta = I_6,\ \theta\,' = I_7,\ \theta\,'' = I_7^{'},$$
$$\psi = I_8,\ \psi\,' = I_9,\ \psi\,'' = I_9^{'},\ \chi = I_{10},\ \chi\,' = I_{11},\ \chi\,'' = I_{11}^{'}.$$

The reduced system of the first-order ODE is given by:

$$I_1\,' = I_2,\ I_2^{'} = \left(\frac{A_2}{A_1}\right)\left(I_1{}^2 - I_3{}^2 - S^2 + I_2 I_5\right) + \left(\frac{A_3}{A_1}\right) M\,(I_1 - S)\,,$$

$$I_3\,' = I_4,\ I_4^{'} = \left(\frac{A_2}{A_1}\right)(2I_1 I_3 + I_4 I_5) + \left(\frac{A_3}{A_1}\right) M\ I_3,\ I_5^{'} = -2I_1,$$

$$I_6\,' = I_7,\ I_7^{'} = \left(\frac{Pr}{A_4}\right)\left(A_5 I_5 I_7 - Nb\ I_7 I_9 - Nt\ (I_7)^2\right),$$

$$I_8\,' = I_9,\ I_9^{'} = Le\ Pr\ I_5 I_9 + Le\ Pr\ Kr\ I_8 - \left(\frac{Nt}{Nb}\right) I_7^{'},$$

$$I_{10}\,' = I_{11},\ I_{11}^{'} = Lb\ Pr\ I_5 I_{11} + Pe\ \left((I_{10} + \Omega)\, I_9^{'} + I_9 I_{11}\right).$$

with

$$I_1(0) = 1,\ I_3(0) = \omega\ ,\ I_5(0) = 0,\ I_6(0) = 1 - S_1,\ I_8(0) = 1 - S_2,$$
$$I_{10}(0) = 1 - S_3,\ I_1(\infty) \to S,\ I_3(\infty) \to 0,\ I_6(\infty) \to 0,\ I_8(\infty) \to 0,\ I_{10}(\infty) \to 0.$$

Since the flow fields satisfy the boundary conditions asymptotically and also since there are no perceptible changes in the results when using larger values for the similarity variable, the conditions at infinity are scaled to 3. The transmuted set of first-order ODEs is resolved using the *bvp5c* routine, a built-in MATLAB function, with an error tolerance of 10^{-10}. The *bvp5c* routine is an efficient numerical scheme that executes a code based on the finite-difference algorithm which utilizes the four-step sixth-order Lobatto IIIA formula. The *bvp5c* routine directly solves the algebraic equations and examines the true error. This process is continued until the appropriate level of error tolerance is reached. The reliability and the accuracy of the proposed numerical technique have been adjudged through a restrictive correspondence with the already published work of Mustafa et al., 2016. For this, the results of $F'(0)$ and $-G'(0)$ are compared when M and ω values are augmented (see Table 8.1).

Table 8.1: Resemblance of $F'(0)$ and $-G'(0)$ with the work of Mustafa et al., 2016 when $S = \phi = Nt = Le = Lb = \Omega = Pe = Kr = S_1 = S_2 = S_3 = 0,\ Nb \to 0$, and $Pr = 1$

M	ω	**Mustafa et al., 2016**		**Present Study**	
		$\mathbf{F'(0)}$	$\mathbf{-G'(0)}$	$\mathbf{F'(0)}$	$\mathbf{-G'(0)}$
0	0	-1.1737	0	-1.173779499	0
	1	-0.9483	1.487	-0.948365298	1.486962505
	2	-0.3263	3.1278	-0.326275283	3.127830777
2	0	-1.8305	0	-1.830489699	0
	1	-1.6635	2.0239	-1.663452576	2.02394492
	2	-1.1754	4.1135	-1.175347049	4.11349385

Table 8.2: Thermophysical properties of water and magnetite nanoparticles

Property	**Water (base fluid)**	**Fe_3O_4 (nanoparticle)**
$\boldsymbol{\rho}$	997.1	5180
$\boldsymbol{C_p}$	4179	670
$\boldsymbol{k}$	0.613	9.7
$\boldsymbol{\sigma}$	0.05	25000

8.4 Results & Discussion

The consequence of pertinent parameters on the flow profiles and the physical quantities are depicted through the contour-styled graphs given in Figures 8.2 - 8.11 and three-dimensional surface plots given in Figures 8.12 - 8.18, respectively. The base values of the dimensionless parameters are chosen as $Pr = 6.2,\ Nt = Nb = 0.05,\ \phi = 0.01,\ \omega = S = \Omega = Kr = 0.5,\ M = 1,\ Le = 2,\ Lb = 0.3,$ and $Pe = S_1 = S_2 = S_3 = 0.1$. In addition, Table 8.2 lists the thermophysical characteristics of water (base fluid) and magnetite nanoparticles.

The positive response of velocity ratio parameter (S) on the radial velocity ($F(\eta)$) and the negative impact of S on the azimuthal velocity ($G(\eta)$) have been graphed in Figures 8.2 and 8.3, respectively. This can be physically associated to the fact that the elongation of the disk weakens the rotational effect causing the velocity to drop in the azimuthal direction whereas the stretching of the disk accelerates the fluid drawn towards the disk causing a rise in the radial velocity. An escalation in the magnetic field parameter (M) causes for the creation of a resistive force (termed Lorentz force) that slows the flow velocities (see Figures 8.4 and 8.5). Figure 8.6 describes the positive deviations in $G(\eta)$ concerning ω (rotation parameter). Physically, an increase in ω enhances the centrifugal force that enlarges the rotational phenomenon of neighbouring fluid layers.

The introduction of magnetite nanoparticles enhances the thermal conductivity of the nanomaterial, raising the nanofluid temperature ($\theta(\eta)$) profile (illustrated in Figure 8.7). Figure 8.8 depicts the decreasing nature of $\theta(\eta)$ with S_1 (thermal

stratification parameter). Physically, this is due to the drop in temperature variation between the ambient and fluid surface with augmenting S_1 values.

Increasing Kr (chemical reaction parameter) values intensify the nanoparticle consumption, thereby causing a decline in the nanoparticle volume fraction ($\psi(\eta)$) (see Figure 8.9). Figure 8.10 elucidates the negative deviation in $\psi(\eta)$ with respect to S_2 (solutal stratification parameter). This decline in $\psi(\eta)$ with mounting values of S_2 can be physically attributed to the decrease in the volumetric fraction between the surface and reference nanoparticles. From Figure 8.11, it can be perceived that the microbial concentration ($\chi(\eta)$) descends with mounting values of S_3 (microbial stratification parameter). This is because an increase in S_3 descends the microbial concentration difference between the surface and away from the surface.

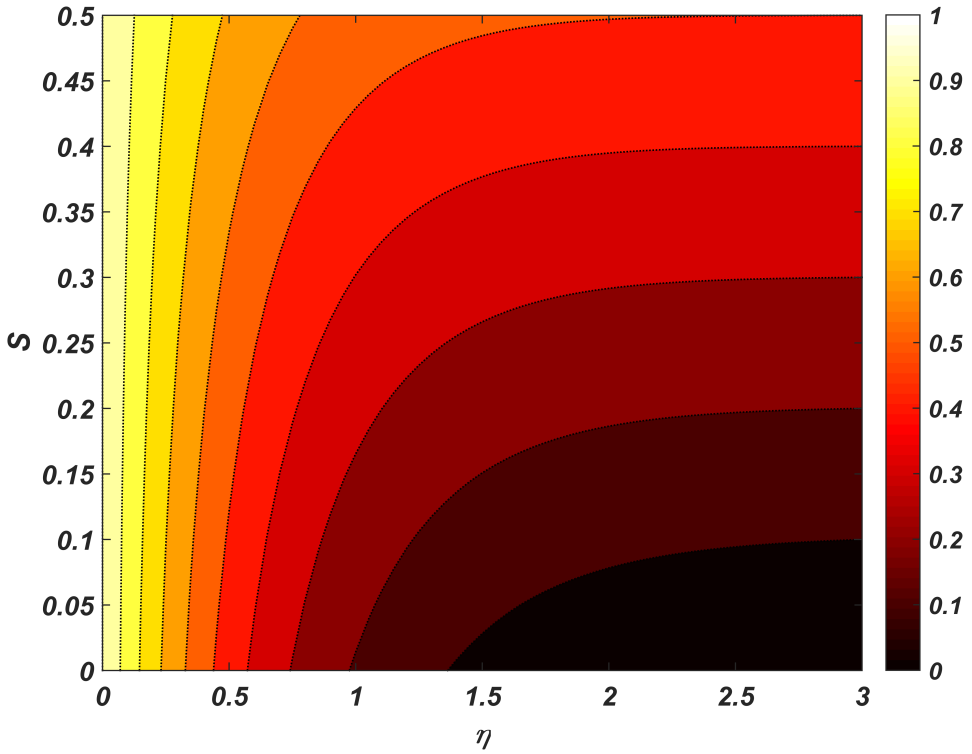

Figure 8.2: Impression of S on $F(\eta)$

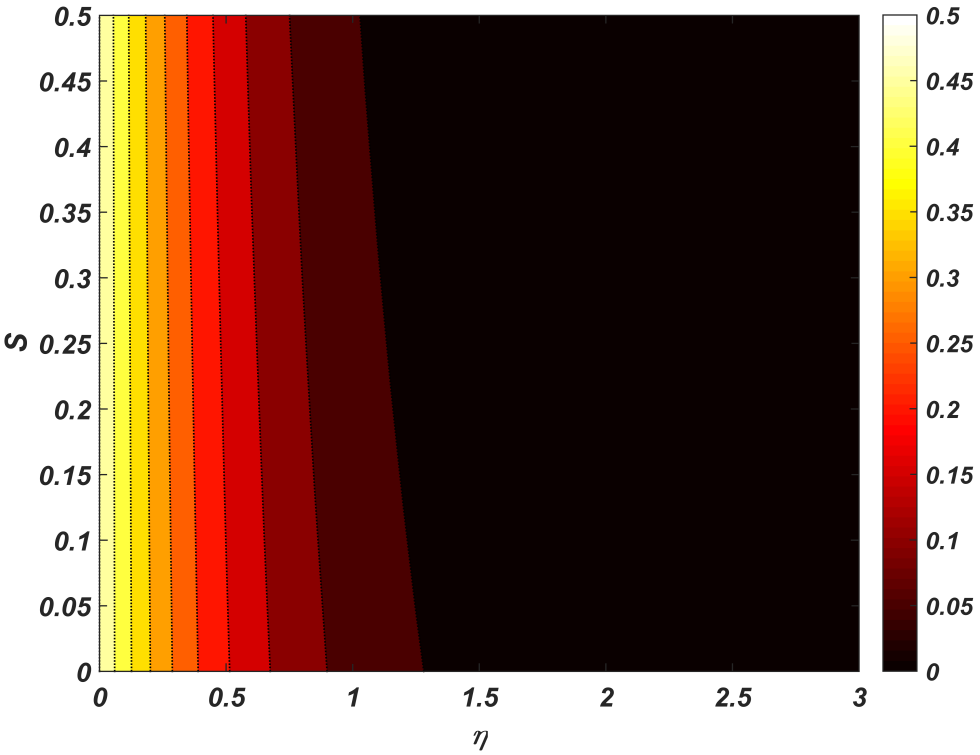

Figure 8.3: Impression of S on $G(\eta)$

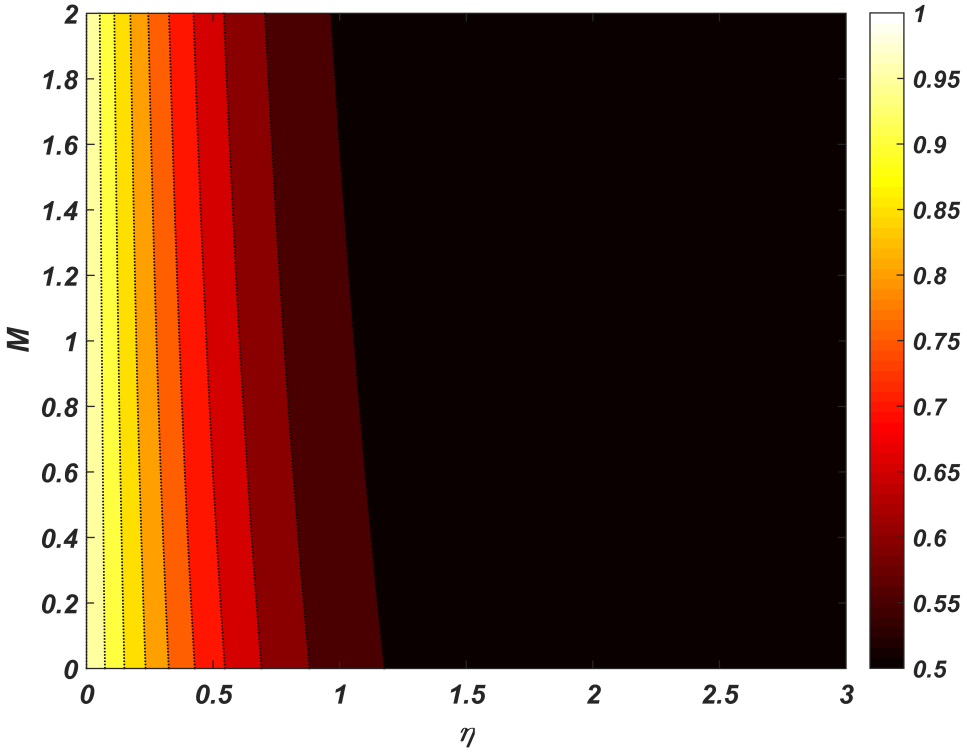

Figure 8.4: Impression of M on $F(\eta)$

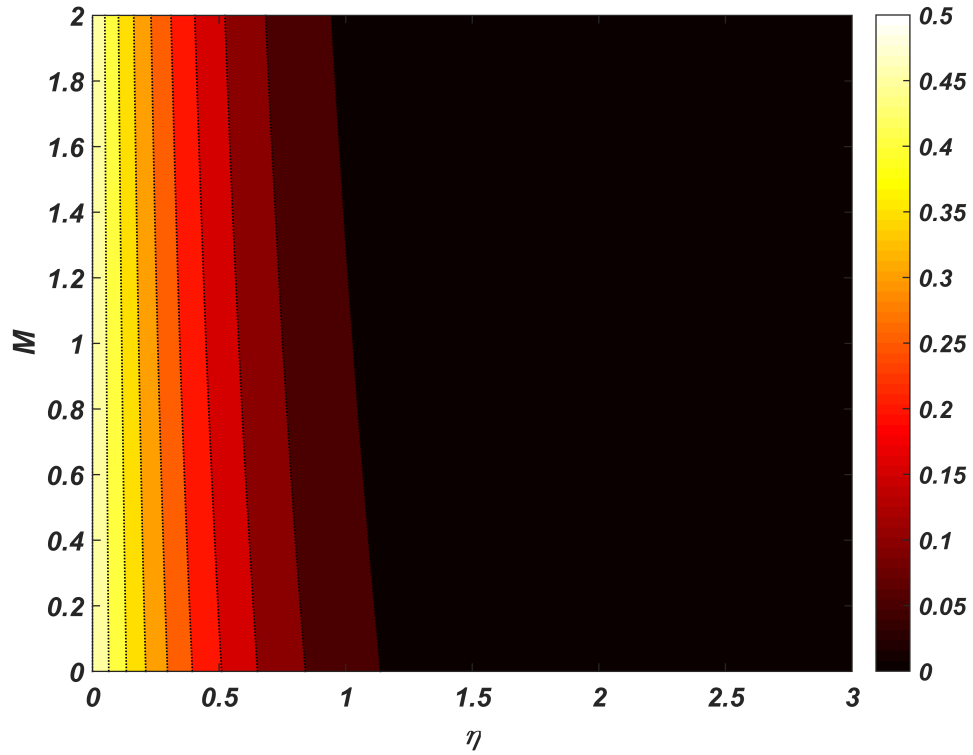

Figure 8.5: Impression of M on $G(\eta)$

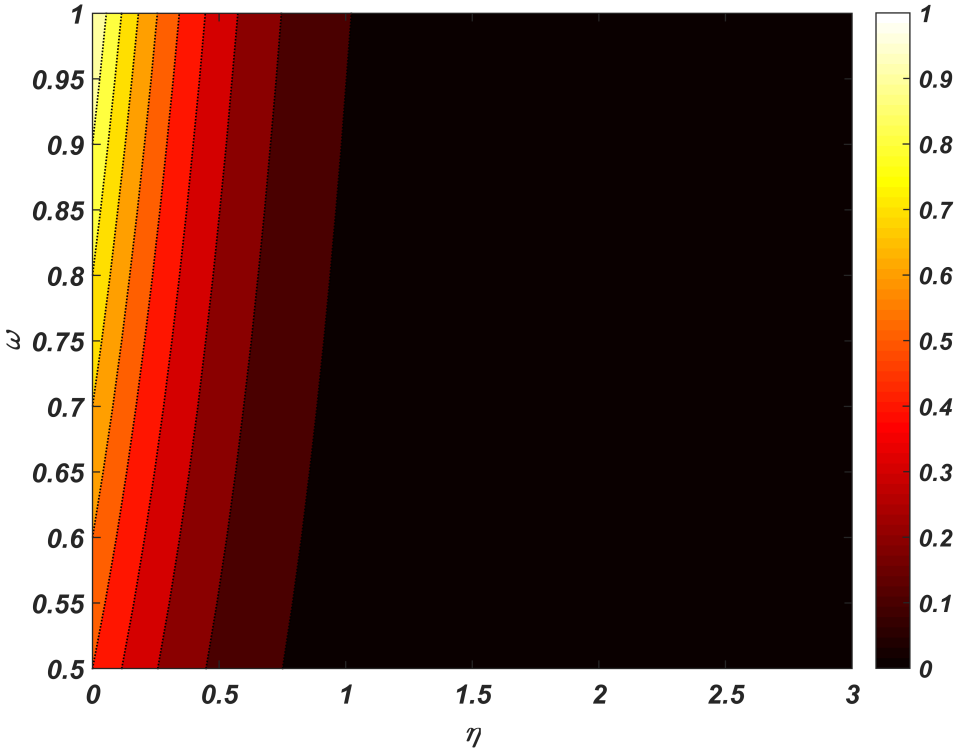

Figure 8.6: Impression of ω on $G(\eta)$

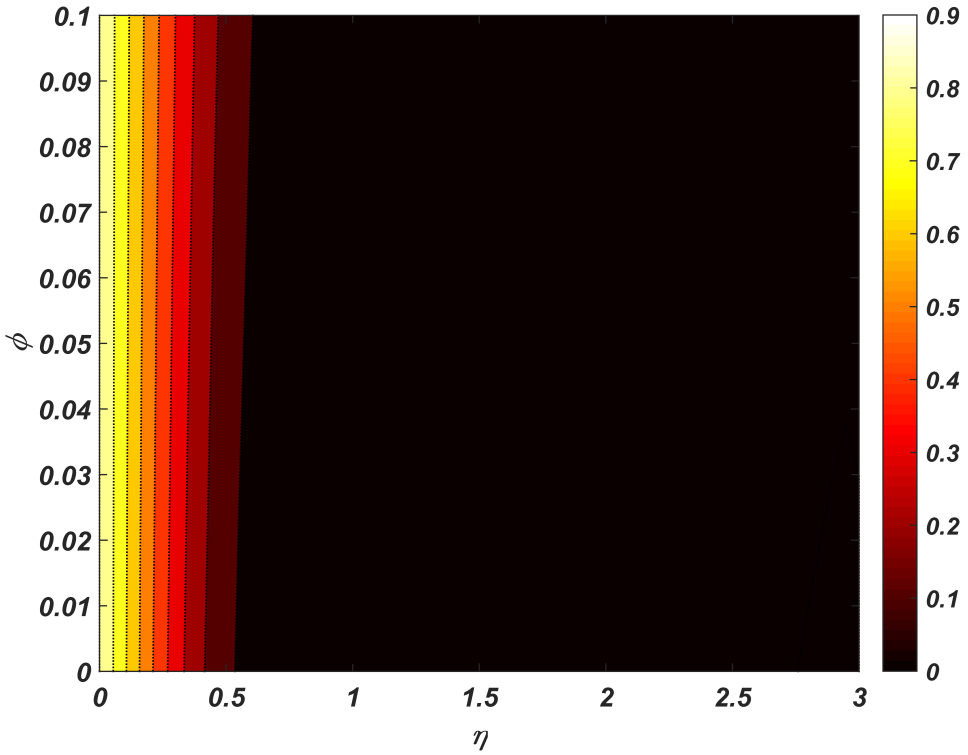

Figure 8.7: Impression of ϕ on $\theta(\eta)$

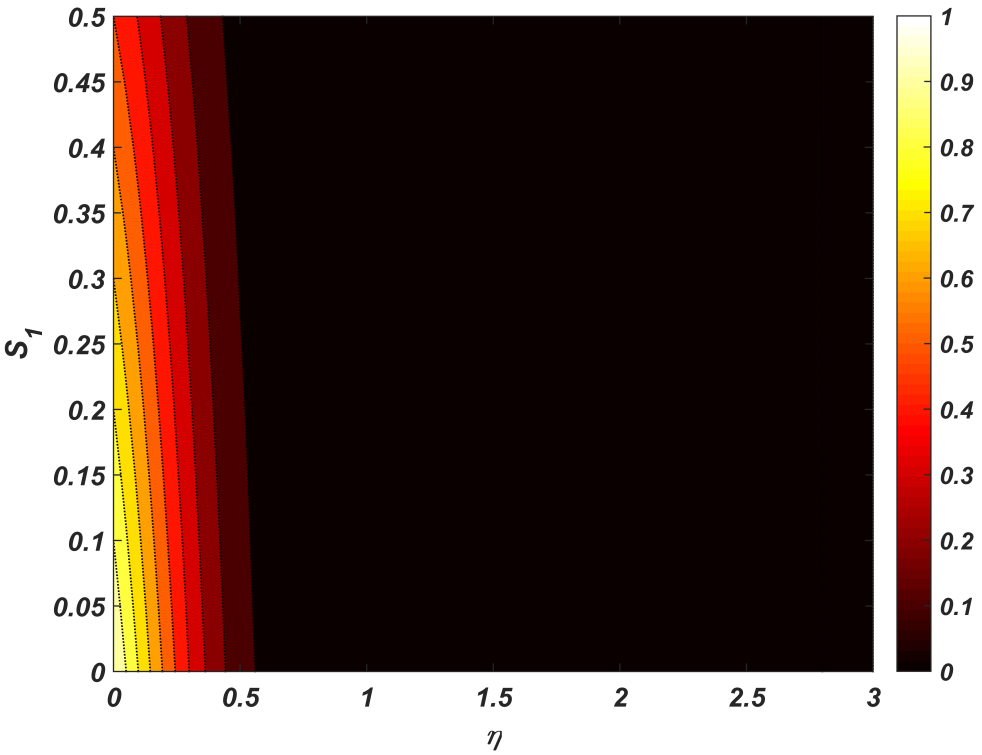

Figure 8.8: Impression of S_1 on $\theta(\eta)$

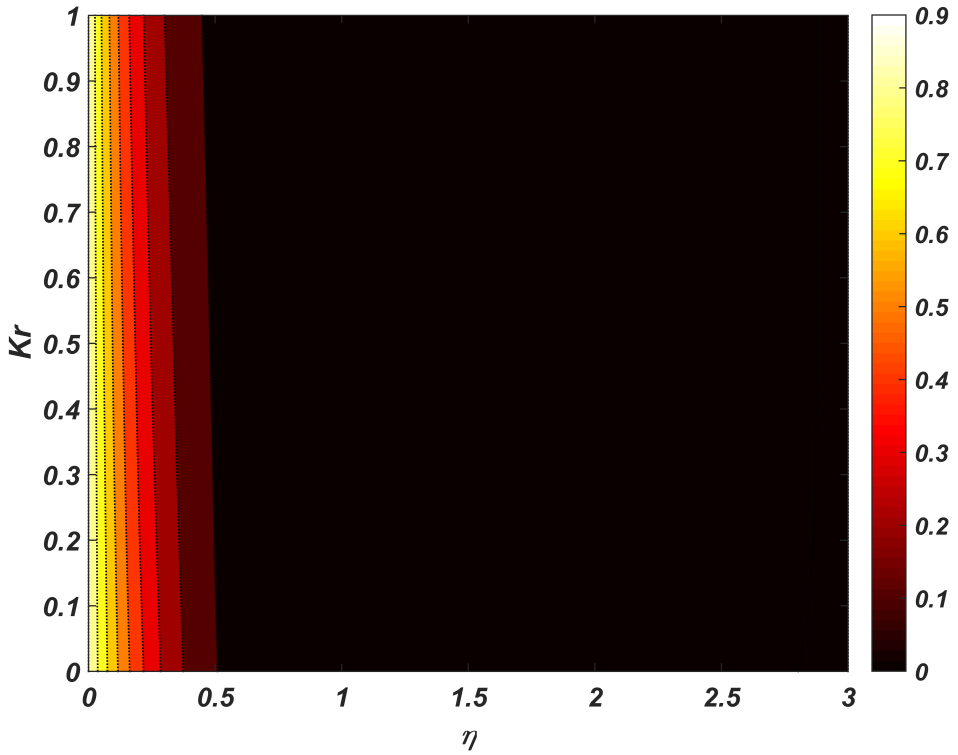

Figure 8.9: Impression of Kr on $\psi(\eta)$

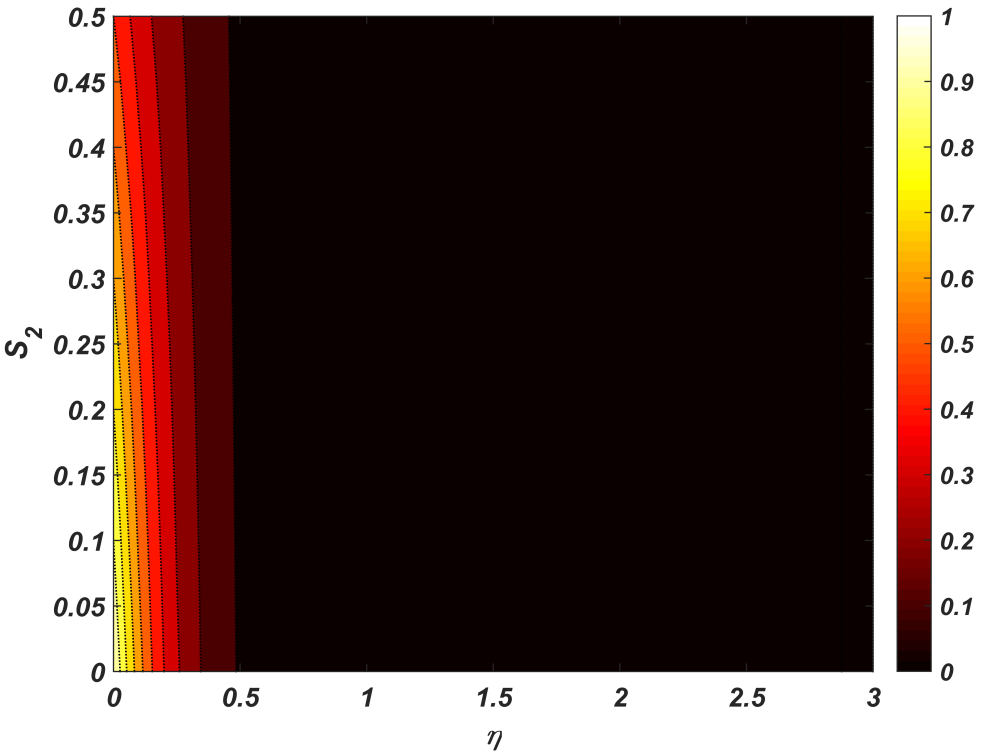

Figure 8.10: Impression of S_2 on $\psi(\eta)$

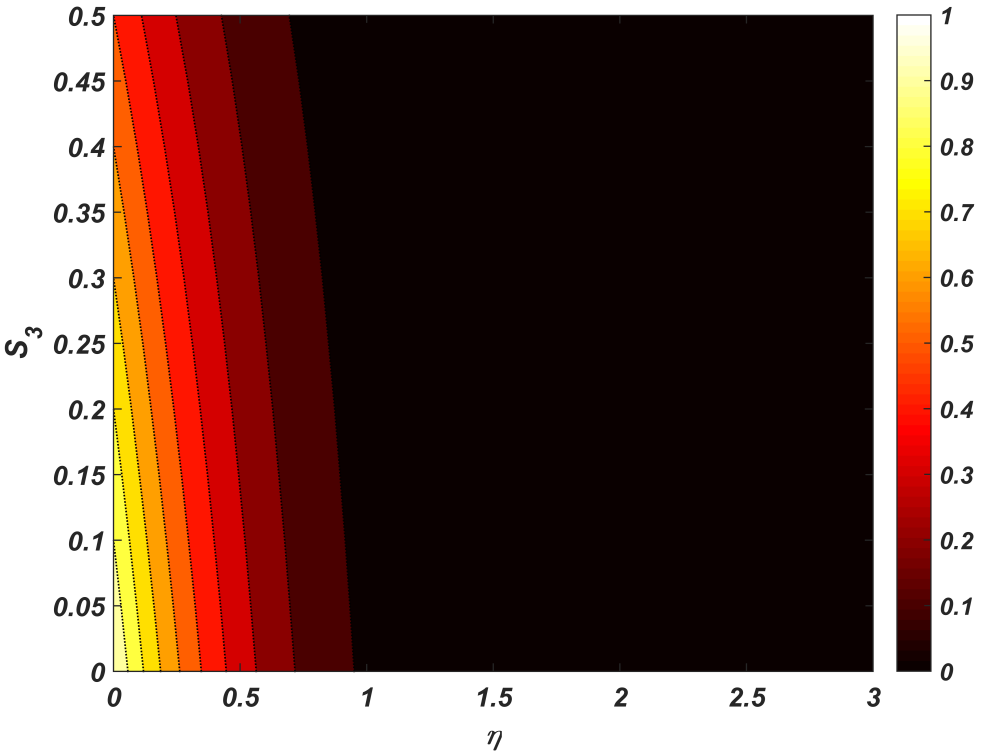

Figure 8.11: Impression of S_3 on $\chi(\eta)$

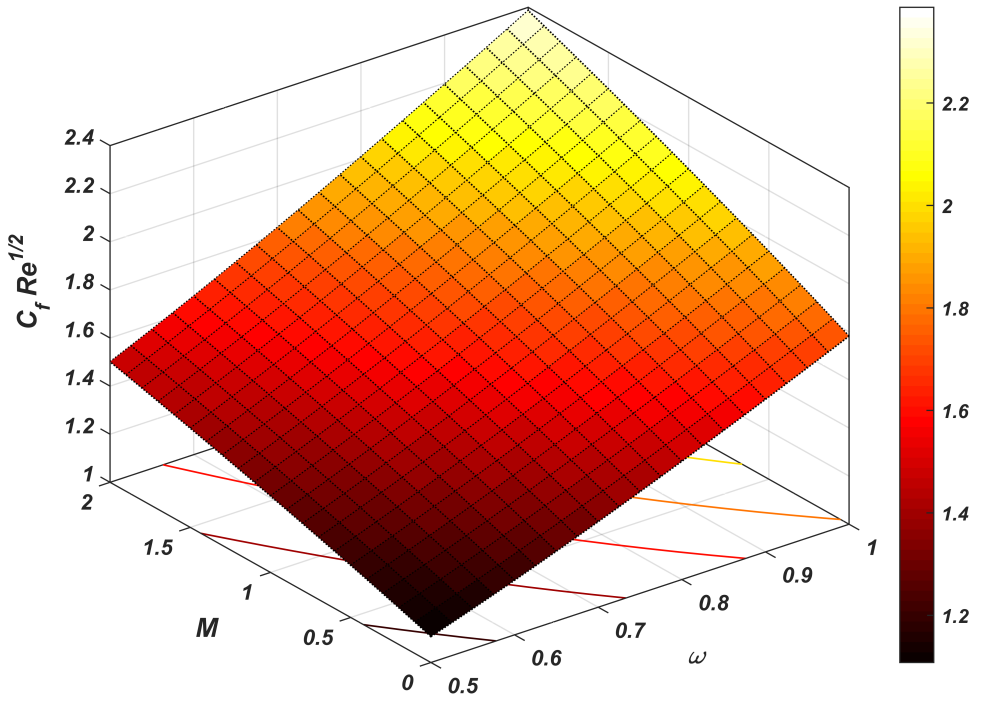

Figure 8.12: Simultaneous impression of ω and M on $C_f\ Re^{1/2}$

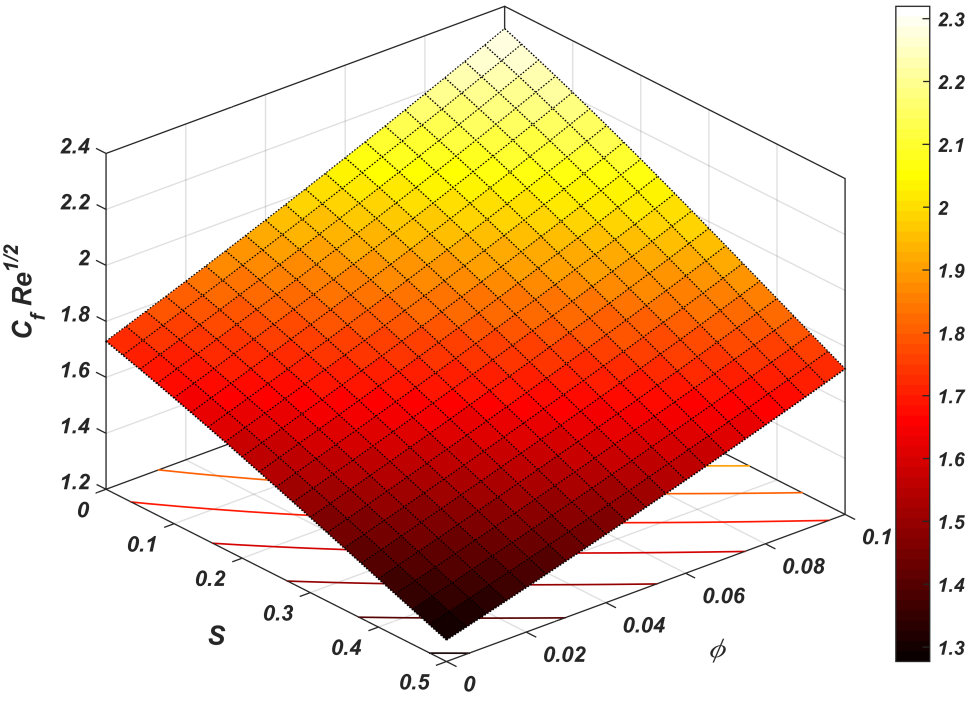

Figure 8.13: Simultaneous impression of ϕ and S on $C_f\ Re^{1/2}$

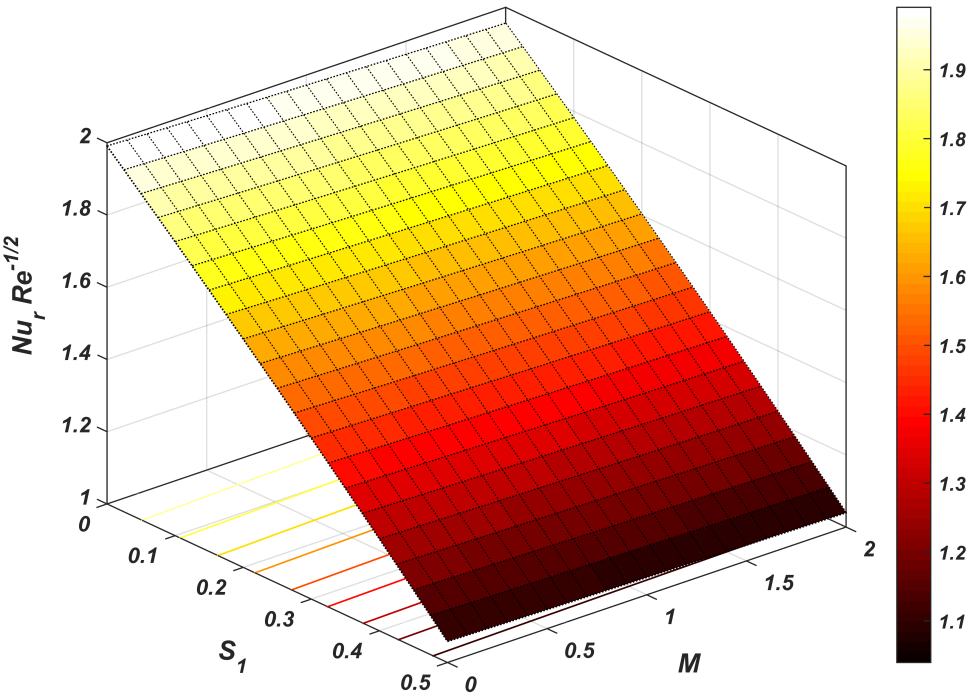

Figure 8.14: Simultaneous impression of S_1 and M on $Nu_r\ Re^{-1/2}$

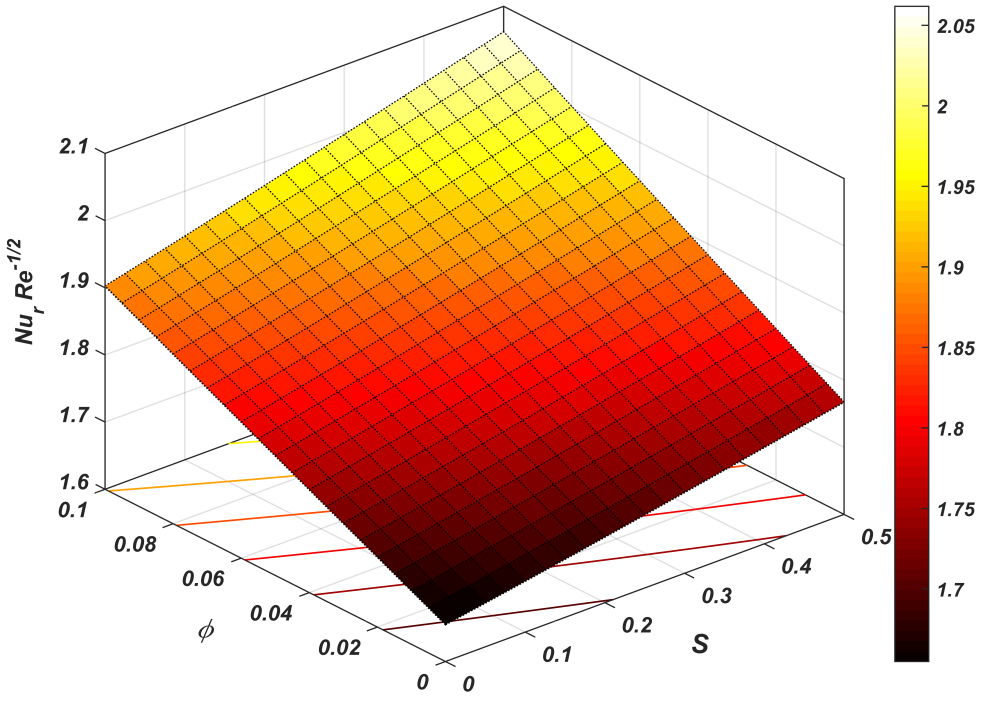

Figure 8.15: Simultaneous impression of ϕ and S on $Nu_r\ Re^{-1/2}$

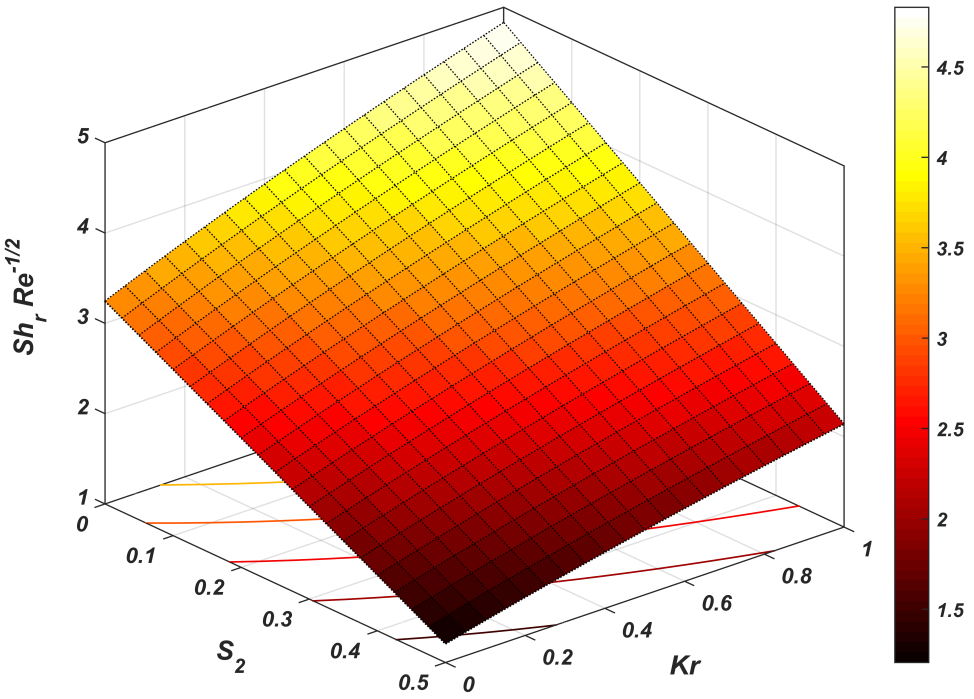

Figure 8.16: Simultaneous impression of S_2 and Kr on $Sh_r\ Re^{-1/2}$

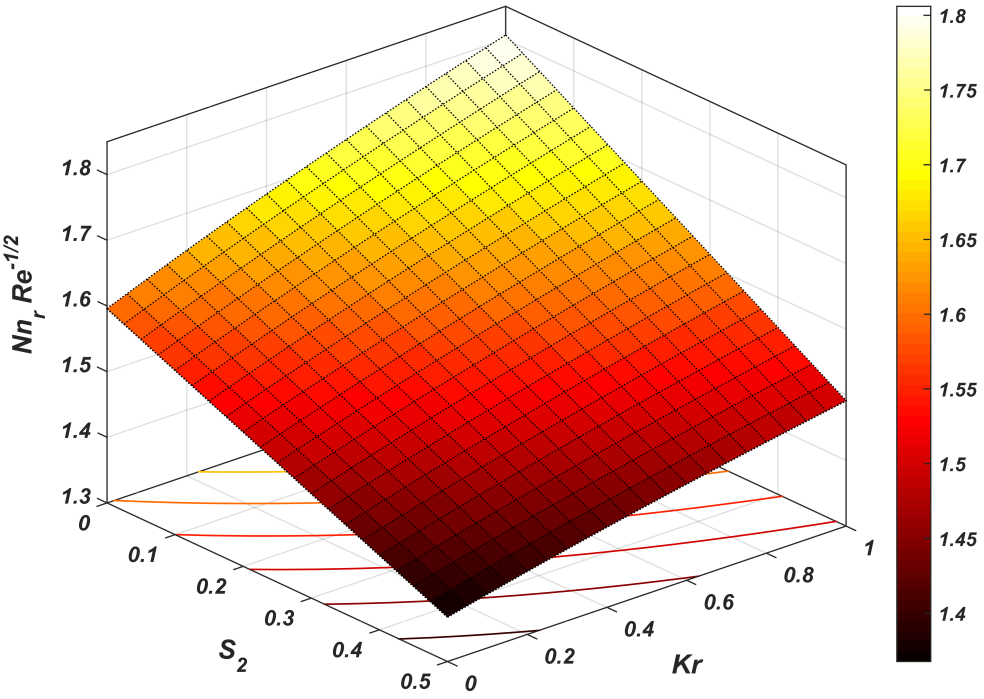

Figure 8.17: Simultaneous impression of S_2 and Kr on $Nn_r\ Re^{-1/2}$

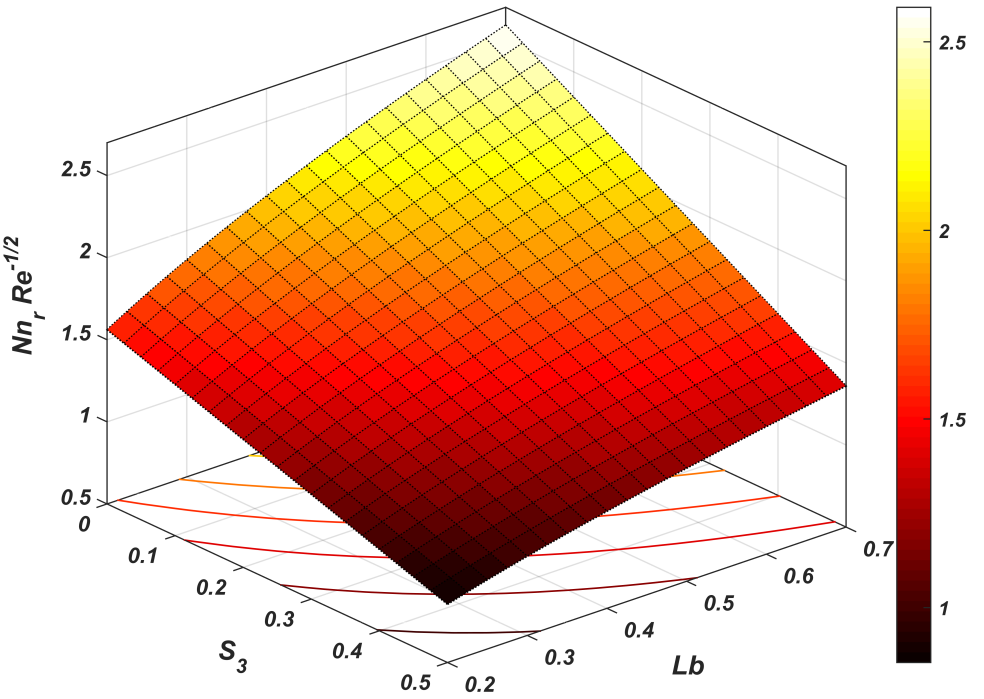

Figure 8.18: Simultaneous impression of S_3 and Lb on $Nn_r\ Re^{-1/2}$

The simultaneous outcome of influential parameters on the physical quantities is depicted with the aid of surface plots (see Figures 8.12 - 8.18). The key observations are:

- Skin friction coefficient $\left(C_f\ Re^{1/2}\right)$ is a decreasing function of S and an increasing function of $\omega,\ M$, and ϕ.
- Highest heat transport $\left(Nu_r\ Re^{-1/2}\right)$ is observed for curtailing values of M and S_1.
- The heat transfer rate ascends with an increase in S and ϕ values.
- Highest mass transfer rate $\left(Sh_r\ Re^{-1/2}\right)$ is observed for curtailed values of S_2 and augmented values of Kr.
- The motile microorganism density number $\left(Nn_r\ Re^{-1/2}\right)$ is an increasing function of Kr and Lb (bioconvection Lewis number).
- $Nn_r\ Re^{-1/2}$ descends with an increase in S_2 and S_3 values.

8.5 Statistical Frame

The four-factor response surface methodology (RSM) is a statistical mechanism that analyzes the mutual response of four independent variables on a dependent variable. In this problem, the impact of magnetic field parameter ($0.2 \leq M \leq 1.8$), thermal stratification parameter ($0.1 \leq S_1 \leq 0.5$), volume fraction of magnetite nanoparticles ($0.01 \leq \phi \leq 0.09$), and velocity ratio parameter ($0.1 \leq S \leq 0.5$) on the heat transport $\left(Nu_r\ Re^{-1/2}\ \right)$ is scrutinized statistically using the Design-Expert software (see Alben, 2002; Montgomery, 2010) and a five-level four-factor response surface optimized model. The effectual parameters and their levels are displayed in Table 8.3.

Table 8.3: Effectual parameter levels

Parameter	**Symbol**	**Levels**				
		$-\mathbf{2}\,(-\alpha)$	**-1 (low)**	**0 (medium)**	**1 (high)**	$\mathbf{2}\,(+\alpha)$
M	$\mathbb{A}$	0.2	0.6	1	1.4	1.8
S_1	$\mathbb{B}$	0.1	0.2	0.3	0.4	0.5
ϕ	$\mathbb{C}$	0.01	0.03	0.05	0.07	0.09
S	$\mathbb{D}$	0.1	0.2	0.3	0.4	0.5

The four-factor response surface optimized model (espousing CCD) for response variable involving linear, quadratic, and interactive terms is couched by:

$$\text{Response} = \mathbb{k}_0 + \mathbb{k}_1\ \mathbb{A} + \mathbb{k}_2\ \mathbb{B} + \mathbb{k}_3\ \mathbb{C} + \mathbb{k}_4\ \mathbb{D} + \mathbb{k}_5\ \mathbb{A}^2 + \mathbb{k}_6\ \mathbb{B}^2 + \mathbb{k}_7\ \mathbb{C}^2 + \mathbb{k}_8\ \mathbb{D}^2 + \mathbb{k}_9\ \mathbb{A}\ \mathbb{B} + \mathbb{k}_{10}\ \mathbb{A}\ \mathbb{C} + \mathbb{k}_{11}\ \mathbb{A}\ \mathbb{D} + \mathbb{k}_{12}\ \mathbb{B}\ \mathbb{C} + \mathbb{k}_{13}\ \mathbb{B}\ \mathbb{D} + \mathbb{k}_{14}\ \mathbb{C}\ \mathbb{D}$$

where $\mathbb{k}_i\ \ (i = 0, 1, \ldots, 14)$ portrays the regression coefficients. The experimental design and the response for the 30 runs (in line with the four-factor CCD) are showcased in Table 8.4.

Table 8.5 (ANOVA table) explains the coherence of the approximated model. A parameter is asserted to be significant if the corresponding p-value is less than 0.05 and the corresponding F-value is greater than 1. It is noticed that the quadratic term in ϕ is not significant for $Nu_r\ Re^{-1/2}$ and hence the term is deleted from the model. The coefficient of determination (R^2) for the model is estimated to be 99.99% which also boosts the model's reliability. The reliability and accuracy of the estimated heat transfer rate model are further elucidated using residual versus predicted plot (see Figure 8.19). Further, a maximum error of 0.0008 is noted from Figure 8.19 which also accounts for the correctness of the model.

The fitted quadratic model is given by:

$$\begin{aligned} Nu_r\ Re^{-1/2}\ (in\ coded\ form) &= 1.47729 - 0.00927\mathbb{A} - 0.19447\mathbb{B} + 0.04253\mathbb{C} \\ &+ 0.02185\mathbb{D} + 0.00035\mathbb{A}^2 - 0.00227\mathbb{B}^2 + 0.00021\mathbb{D}^2 + 0.00123\mathbb{A}\mathbb{B} - 0.00043\mathbb{A}\mathbb{C} \\ &+ 0.00218\mathbb{A}\mathbb{D} - 0.00628\mathbb{B}\mathbb{C} - 0.00286\mathbb{B}\mathbb{D} + 0.00147\mathbb{C}\mathbb{D} \end{aligned} \tag{8.5.1}$$

$$Nu_r\ Re^{-1/2}\ (in\ actual\ form) = 1.85770 - 0.05044M - 1.59627S_1 + 2.86282\phi + 0.20021S + 0.00220M^2 - 0.22688{S_1}^2 + 0.02123S^2 + 0.03065MS_1 - 0.05408M\phi + 0.05459MS - 3.14150S_1\phi - 0.28623S_1S + 0.73642\phi S \quad (8.5.2)$$

The fitted model (Equations (8.5.1) and (8.5.2)) reveals that S_1 and M reduce whereas ϕ and S increase the heat transfer rate. The parallel effect of two parameters on the heat transfer rate is delineated using surface plots (see Figure 8.20) by anchoring the remaining two parameters at their corresponding median level. From Figure 8.20, it is inferred that the heat transfer rate is highest for curtailed values of S_1 & M and augmented values of ϕ & S.

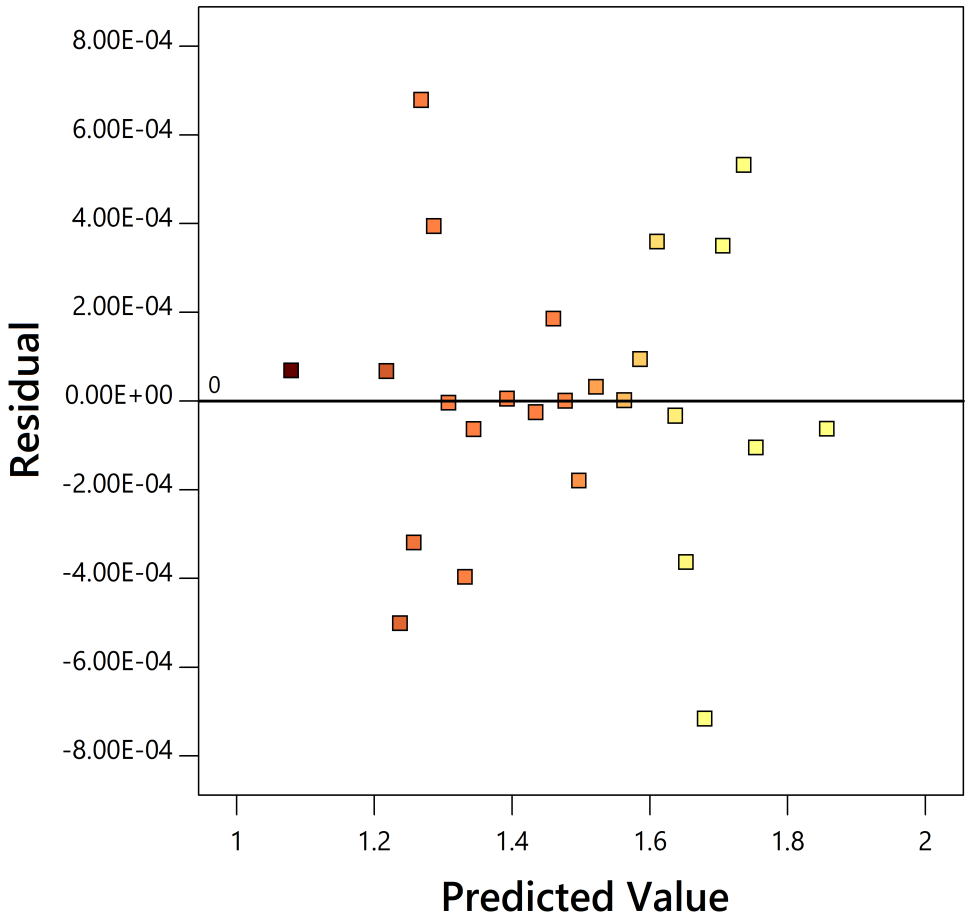

Figure 8.19: Residual versus Predicted value

Table 8.4: Four-factor CCD experimental design and the corresponding responses

Run	M	S_1	ϕ	S	$Nu_r\ Re^{-1/2}$
1	0.6 (-1)	0.2 (-1)	0.03 (-1)	0.2 (-1)	1.610761713
2	1.4 (1)	0.2 (-1)	0.03 (-1)	0.2 (-1)	1.585998024
3	0.6 (-1)	0.4 (1)	0.03 (-1)	0.2 (-1)	1.236802131
4	1.4 (1)	0.4 (1)	0.03 (-1)	0.2 (-1)	1.217775854
5	0.6 (-1)	0.2 (-1)	0.07 (1)	0.2 (-1)	1.70630398
6	1.4 (1)	0.2 (-1)	0.07 (1)	0.2 (-1)	1.679008737
7	0.6 (-1)	0.4 (1)	0.07 (1)	0.2 (-1)	1.307718566
8	1.4 (1)	0.4 (1)	0.07 (1)	0.2 (-1)	1.286791893
9	0.6 (-1)	0.2 (-1)	0.03 (-1)	0.4 (1)	1.652149555
10	1.4 (1)	0.2 (-1)	0.03 (-1)	0.4 (1)	1.636715167
11	0.6 (-1)	0.4 (1)	0.03 (-1)	0.4 (1)	1.268642663
12	1.4 (1)	0.4 (1)	0.03 (-1)	0.4 (1)	1.256785193
13	0.6 (-1)	0.2 (-1)	0.07 (1)	0.4 (1)	1.753850765
14	1.4 (1)	0.2 (-1)	0.07 (1)	0.4 (1)	1.736993024
15	0.6 (-1)	0.4 (1)	0.07 (1)	0.4 (1)	1.344211711
16	1.4 (1)	0.4 (1)	0.07 (1)	0.4 (1)	1.331287872
17	0.2 (-2)	0.3 (0)	0.05 (0)	0.3 (0)	1.49705729
18	1.8 (2)	0.3 (0)	0.05 (0)	0.3 (0)	1.46033275
19	1 (0)	0.1 (-2)	0.05 (0)	0.3 (0)	1.857086312
20	1 (0)	0.5 (2)	0.05 (0)	0.3 (0)	1.07934181
21	1 (0)	0.3 (0)	0.01 (-2)	0.3 (0)	1.392855907
22	1 (0)	0.3 (0)	0.09 (2)	0.3 (0)	1.562984781
23	1 (0)	0.3 (0)	0.05 (0)	0.1 (-2)	1.434411677
24	1 (0)	0.3 (0)	0.05 (0)	0.5 (2)	1.521865896
25	1 (0)	0.3 (0)	0.05 (0)	0.3 (0)	1.477286276
26	1 (0)	0.3 (0)	0.05 (0)	0.3 (0)	1.477286276
27	1 (0)	0.3 (0)	0.05 (0)	0.3 (0)	1.477286276
28	1 (0)	0.3 (0)	0.05 (0)	0.3 (0)	1.477286276
29	1 (0)	0.3 (0)	0.05 (0)	0.3 (0)	1.477286276
30	1 (0)	0.3 (0)	0.05 (0)	0.3 (0)	1.477286276

Table 8.5: ANOVA table

Source	**Deg. of freedom**	**Sum of squares**	**Mean squares**	**F-Value**	**p-Value**
Model	14	0.9656	0.069	4.29E+05	< 0.0001
M	1	0.0021	0.0021	12834.51	< 0.0001
S_1	1	0.9076	0.9076	5.65E+06	< 0.0001
ϕ	1	0.0434	0.0434	2.70E+05	< 0.0001
S	1	0.0115	0.0115	71266.13	< 0.0001
$M * S_1$	1	0	0	149.6	< 0.0001
$M * \phi$	1	2.99E-06	2.99E-06	18.63	0.0006
$M * S$	1	0.0001	0.0001	474.55	<0.0001
$S_1 * \phi$	1	0.0006	0.0006	3928.7	<0.0001
$S_1 * S$	1	0.0001	0.0001	815.36	< 0.0001
$\phi * S$	1	0	0	215.89	< 0.0001
$M * M$	1	3.39E-06	3.39E-06	21.07	0.0004
$S_1 * S_1$	1	0.0001	0.0001	878.23	< 0.0001
$\phi * \phi$	1	6.82E-07	6.82E-07	**4.24**	**0.0572**
$S * S$	1	1.24E-06	1.24E-06	7.69	0.0142
Residual	15	2.41E-06	1.61E-07		
Lack-of-Fit	10	2.41E-06	2.41E-07	*	*
Pure Error	5	0	0		
Total	29	0.9656			
$R^2 = 0.9999975$			Adjusted $R^2 = 0.9999952$		

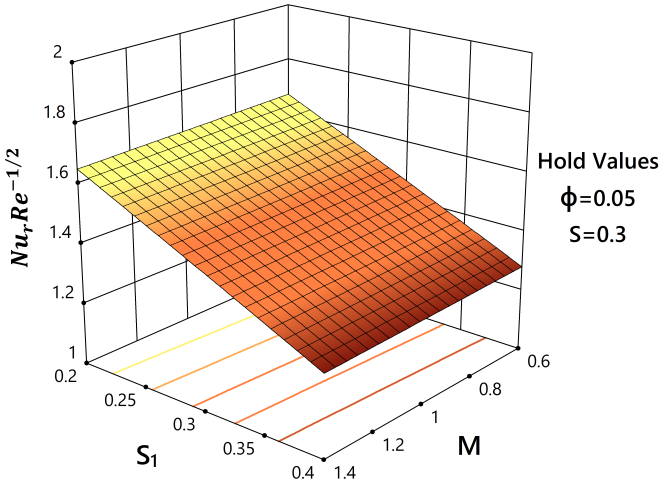

(a)

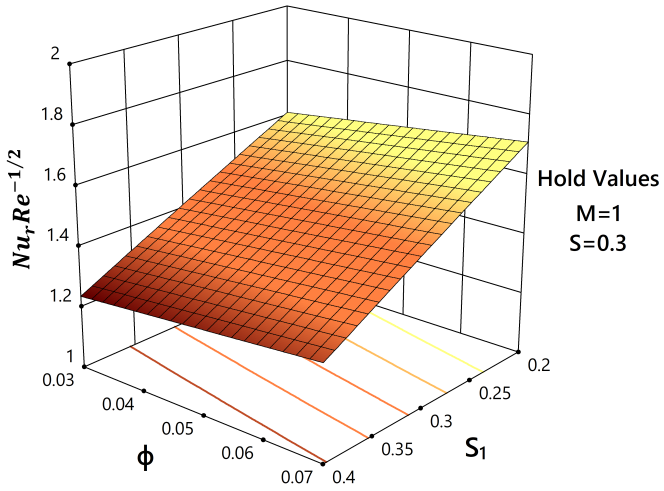

(b)

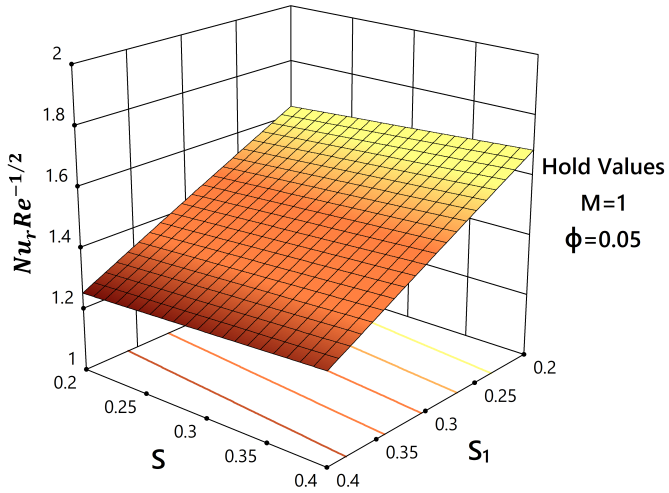

(c)

Figure 8.20: Surface plots for $Nu_r\ Re^{-1/2}$

8.6 Conclusion

In view of its practical application in pharmaceuticals, biosensors, medical instruments, bio-chromatography, microchip pump, biomedical science, micro-actuators, and aerodynamics, the significance of magnetic field and stratification effects on the bioconvective stagnation-point flow over a whirling stretchable disk has been numerically simulated with the help of the finite-difference based *bvp5c* routine. The nanofluid flow has been modelled using MBNM. Further, the impact of magnetic field parameter ($0.2 \leq M \leq 1.8$), thermal stratification parameter ($0.1 \leq S_1 \leq 0.5$), volume fraction of magnetite nanoparticles ($0.01 \leq \phi \leq 0.09$), and velocity ratio parameter ($0.1 \leq S \leq 0.5$) on the heat transport has been scrutinized statistically using a five-level four-factor response surface optimized model. The major conclusions of the present study are:

- The magnetic field parameter has a destructive effect on the radial and azimuthal velocity profiles.
- The drag coefficient increases and the heat transfer rate decreases with growing values of magnetic field parameter.
- Increments in the velocity ratio parameter tend to escalate and curtail the radial velocity and the azimuthal velocity profiles, respectively.
- The nanofluid temperature elevates with an increase in the volume fraction of magnetite nanoparticles and depletes with augmentation in the thermal stratification parameter.
- The solutal and microbial stratification parameters have a negative effect on the nanoparticle volume fraction and the microbial concentration, respectively.
- Augmentation in the chemical reaction parameter increases the nanoparticle consumption, thereby reducing the nanoparticle volume fraction.
- The motile microorganism density number descends with ascending values of solutal and microbial stratification parameters.
- The heat transport is negatively correlated with the thermal stratification parameter and the magnetic field parameter.

Appendix I: Non-dimensional qunatities

$M = \frac{\sigma_f \ B_0^2}{\rho_f \ \mathrm{c}}$	Magnetic field parameter
$S = \frac{a}{c}$	Velocity ratio parameter
$\omega = \frac{\Lambda}{c}$	Rotation parameter
$Nb = \frac{\tau \ D_B \ (C_w - C_0)}{\vartheta_f}$	Brownian motion parameter
$Nt = \frac{\tau \ D_T \ (T_w - T_0)}{T_\infty \ \vartheta_f}$	Thermophoresis parameter
$Pr = \frac{(\mu C_p)_f}{k_f} = \frac{\vartheta_f}{\alpha_f}$	Prandtl number
$Kr = \frac{k_r}{c}$	Chemical reaction parameter
$\tau = \frac{(\rho \ C_P)_p}{(\rho \ C_P)_f}$	Effective heat capacity ratio
$Le = \frac{\alpha_f}{D_B}$	Lewis number
$Lb = \frac{\alpha_f}{D_m}$	Bioconvection Lewis number
$Pe = \frac{bW_c}{D_m}$	Bioconvection Peclet number
$\Omega = \frac{N_\infty}{N_w - N_0}$	Microorganism concentration difference parameter
$S_1 = \frac{\delta_2}{\delta_1}$	Thermal stratification parameter
$S_2 = \frac{\epsilon_2}{\epsilon_1}$	Solutal stratification parameter
$S_3 = \frac{\zeta_2}{\zeta_1}$	Motile density stratification parameter

Appendix II: Nomenclature

a, c, Λ	Positive constants	W_c	Maximum cell swimming speed
u, v, w	Velocity components	B_0	Strength of magnetic field
Nn_r	Local motile density	T_∞	Ambient fluid temperature
T_0	Reference temperature	N_∞	Ambient microbial concentration
C	Fluid concentration	C_0	Reference nanoparticle concentration
T	Fluid temperature	N_0	Reference microbial concentration
r, φ, z	Polar coordinates	N_w	Microbial concentration near wall
b	Chemotaxis constant	C_w	Nanoparticle concentration near wall
T_w	Wall fluid temperature	C_∞	Ambient nanoparticle concentration
ρC_p	Heat capacity	C_f	Local drag coefficient
k_r	Reaction rate constant	Nu_r	Local Nusselt number
Sh_r	Local Sherwood number	N	Microorganism concentration
σ	Electrical conductivity	μ	Dynamic viscosity
η	Dimensionless variable	D_B	Chemical molecular diffusivity
ϑ	Kinematic viscosity	D_m	Microorganism diffusion coefficient
$\delta_i, \epsilon_i, \zeta_i$	Dimensional constants	D_T	Thermophoretic diffusion coefficient
k	Thermal conductivity	u_e, v_e	Free stream velocity
α	Thermal diffusivity	R^2	Coefficient of determination
ρ	Fluid density	ϕ	Volume fraction of Fe_3O_4